Monthly Notices
of the
ROYAL ASTRONOMICAL SOCIETY

MNRAS **485,** 961–971 (2019)
Advance Access publication 2019 February 13

doi:10.1093/mnras/stz444

The ASAS-SN catalogue of variable stars III: variables in the southern *TESS* continuous viewing zone

T. Jayasinghe [1,2]★ K. Z. Stanek,[1,2] C. S. Kochanek,[1,2] B. J. Shappee,[3] T. W.-S. Holoien [4] Todd A. Thompson,[1,2,5] J. L. Prieto,[6,7] Subo Dong,[8] M. Pawlak,[9] O. Pejcha [9] J. V. Shields,[1] G. Pojmanski,[10] S. Otero,[11] N. Hurst,[12] C. A. Britt[12] and D. Will[1,12]

[1]*Department of Astronomy, The Ohio State University, 140 West 18th Avenue, Columbus, OH 43210, USA*
[2]*Center for Cosmology and Astroparticle Physics, The Ohio State University, 191 W. Woodruff Avenue, Columbus, OH 43210, USA*
[3]*Institute for Astronomy, University of Hawaii, 2680 Woodlawn Drive, Honolulu, HI 96822,USA*
[4]*Carnegie Observatories, 813 Santa Barbara Street, Pasadena, CA 91101, USA*
[5]*Institute for Advanced Study, Princeton, NJ 08540, USA*
[6]*Núcleo de Astronomía de la Facultad de Ingeniería y Ciencias, Universidad Diego Portales, Av. Ejército 441, Santiago, Chile*
[7]*Millennium Institute of Astrophysics, Santiago, Chile*
[8]*Kavli Institute for Astronomy and Astrophysics, Peking University, Yi He Yuan Road 5, Hai Dian District, China*
[9]*Institute of Theoretical Physics, Faculty of Mathematics and Physics, Charles University in Prague, Czech Republic*
[10]*Warsaw University Observatory, Al Ujazdowskie 4, 00-478 Warsaw, Poland*
[11]*The American Association of Variable Star Observers, 49 Bay State Road, Cambridge, MA 02138, USA*
[12]*ASC Technology Services, 433 Mendenhall Laboratory 125 South Oval Mall Columbus, OH 43210, USA*

Accepted 2019 February 11. Received 2019 February 11; in original form 2018 December 31

ABSTRACT

The All-Sky Automated Survey for Supernovae (ASAS-SN) provides long-baseline (∼4 yr) light curves for sources brighter than $V \lesssim 17$ mag across the whole sky. The *Transiting Exoplanet Survey Satellite* (*TESS*) has started to produce high-quality light curves with a baseline of at least 27 d, eventually for most of the sky. The combination of ASAS-SN and *TESS* light curves probes both long- and short-term variability in great detail, especially towards the *TESS* continuous viewing zones (CVZ) at the ecliptic poles. We have produced ∼1.3 million *V*-band light curves covering a total of ∼1000 deg^2 towards the southern *TESS* CVZ and have systematically searched these sources for variability. We have identified ∼11 700 variables, including ∼7 000 new discoveries. The light curves and characteristics of the variables are all available through the ASAS-SN variable stars data base (https://asas-sn.osu.edu/variables). We also introduce an online resource to obtain pre-computed ASAS-SN *V*-band light curves (https://asas-sn.osu.edu/photometry) starting with the light curves of the ∼1.3 million sources studied in this work. This effort will be extended to provide ASAS-SN light curves for ∼50 million sources over the entire sky.

Key words: catalogues – surveys – binaries: eclipsing.

1 INTRODUCTION

The study of stellar variability has been invigorated by the advent of modern large-scale sky surveys in the modern era. Recent surveys such as the All-Sky Automated Survey (ASAS; Pojmanski 2002), the Optical Gravitational Lensing Experiment (OGLE; Udalski 2003), the Northern Sky Variability Survey (NSVS; Woźniak et al. 2004), MACHO (Alcock et al. 1997), EROS (Derue et al. 2002), the Catalina Real-Time Transient Survey (CRTS; Drake et al. 2014), the Asteroid Terrestrial-impact Last Alert System (ATLAS; Heinze et al. 2018; Tonry et al. 2018), and *Gaia* (Gaia Collaboration 2018a; Gaia Collaboration et al. 2018b; Holl et al. 2018) have collectively discovered $\gtrsim 10^6$ variables.

Variable stars are excellent astrophysical probes and have been used in numerous astronomical contexts. Pulsating variables such as Cepheids and RR Lyrae stars are commonly used as distance indicators owing to the period luminosity relationships seen amongst these variables (e.g. Leavitt 1908; Matsunaga et al. 2006; Beaton et al. 2018, and references therein). Eclipsing binary stars are excellent

★ E-mail: jayasinghearachchilage.1@osu.edu

probes of stellar systems and with sufficient radial velocity follow-up, they allow for the derivation of useful astrophysical parameters, including the masses and radii of the stars in these systems (Torres, Andersen & Giménez 2010). Variable stars are also useful for the study of stellar populations and Galactic structure (Feast & Whitelock 2014; Matsunaga 2018) .

Until recently, the All-Sky Automated Survey for SuperNovae (ASAS-SN, Shappee et al. 2014; Kochanek et al. 2017) monitored the visible sky to a depth of $V \lesssim 17$ mag with a cadence of 2–3 d using two units in Chile and Hawaii each with four telescopes. Starting in 2017, ASAS-SN expanded to five units with 20 telescopes. The three new units all started with *g*-band filters and the two original units have now switched to the *g* band as well. The ASAS-SN telescopes are hosted by the Las Cumbres Observatory (LCO; Brown et al. 2013) in Hawaii, Chile, Texas, and South Africa. ASAS-SN primarily focuses on the detection of bright supernovae (e.g. Holoien et al. 2017, 2019), tidal disruption events (e.g. Holoien et al. 2014, 2016, 2018) and other transients (e.g. Rodríguez et al. 2018; Tucker et al. 2018), but its excellent baseline allows for the study of variability amongst the $\gtrsim 50$ million bright ($V < 17$ mag) sources across the whole sky. ASAS-SN team members have also studied the relative specific Type Ia supernovae rates (Brown et al. 2019) and the largest amplitude M-dwarf flares seen in ASAS-SN (Schmidt et al. 2018).

In Paper I (Jayasinghe et al. 2018a), we reported ∼66 000 new variables that were flagged during the search for supernovae, most of which are located in regions close to the Galactic plane or Celestial poles that were not well sampled by previous surveys. In Paper II (Jayasinghe et al. 2018b), we uniformly analysed ∼412 000 known variables from the VSX catalogue and developed a robust variability classifier utilizing the ASAS-SN *V*-band light curves and data from external catalogues. We have also explored the synergy between ASAS-SN and APOGEE (Holtzman et al. 2015) with the discovery of the first likely non-interacting binary composed of a black hole with a field red giant (Thompson et al. 2018) and a detailed variability analysis of the APOGEE sources to identify 1914 periodic variables (Pawlak et al., in preparation). We have also identified rare variables, including two very long-period detached eclipsing binaries (Jayasinghe et al. 2018c,d) and 19 R Coronae Borealis stars (Shields et al. 2018) .

The *Transiting Exoplanet Survey Satellite* (*TESS*; Ricker et al. 2015) will produce a large number of high-quality light curves with a baseline of at least 27 d for most of the sky. The *TESS* input catalogue (TIC; Stassun et al. 2018) contains ∼470 million sources, out of which 200 000 selected targets are observed at a 2 min cadence, while the remaining sources are observed with a cadence of 30 min. Oelkers et al. (2018) recently identified variable sources in a sample of 4 million TIC sources, but did not classify these variables into explicit types. These sources were classified in Paper II using ASAS-SN data.

Sources closer to the *TESS* continous viewing zone (CVZ) will be observed for a substantially longer period, approaching 1 yr and ∼15 000 epochs at the ecliptic poles. These *TESS* light curves will probe short-period variability in great detail. ASAS-SN provides long-baseline ($\gtrsim$4 yr) light curves sampled at a cadence of ∼1–3 d that complement the *TESS* light curves.

We extracted the ASAS-SN light curves of ∼1.3 million sources within 18 deg of the Southern Ecliptic Pole. These sources are within the southern *TESS* CVZ and will have well-sampled *TESS* light curves. In this work, we systematically search this sample for variable sources. This is, in part, a test run for carrying out such a search over the entire sky. In Section 2, we discuss the ASAS-SN observations and data reduction procedures. Section 3 discusses the variability search and classification procedures. In Section 4, we discuss our results and we present a summary of our work in Section 5. All the light curves of these sources are made available to the public through our online data base.

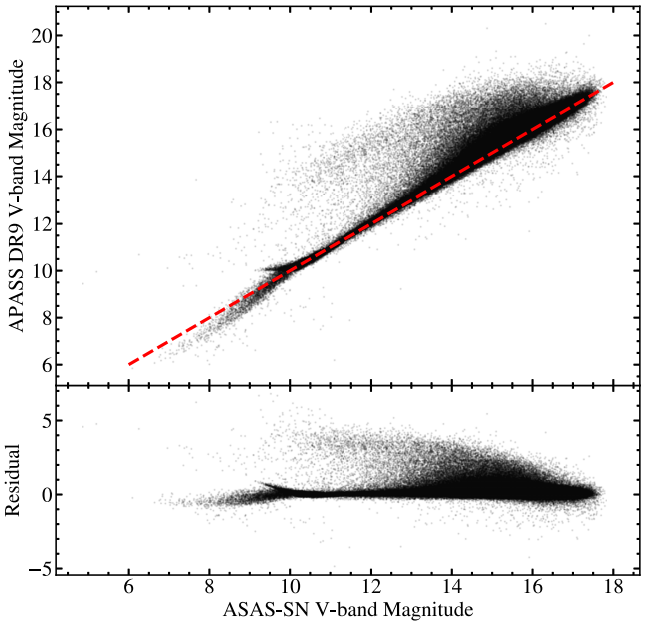

Figure 1. Comparison of the mean ASAS-SN *V*-band magnitudes to the APASS DR9 *V*-band magnitudes. The red dashed line illustrates a perfect calibration.

2 OBSERVATIONS AND DATA REDUCTION

We started with the AAVSO Photometric All-Sky Survey (APASS; Henden et al. 2015) DR9 catalogue as our input source catalogue. We selected all the APASS sources with $V < 17$ mag in all the ASAS-SN fields with central field coordinates within 18 deg from the Southern Ecliptic Pole ($\alpha = 90$ deg, $\delta = -66.55$ deg). This resulted in a list of ∼1.3M sources spanning a total of ∼1000 deg^2. ASAS-SN V-band observations were made by the 'Brutus' (Haleakala, Hawaii) and 'Cassius' (CTIO, Chile) quadruple telescopes between 2013 and 2018. Each ASAS-SN field has ∼ 200–600 epochs of observation to a depth of $V \lesssim 17$ mag. Each camera has a field of view of 4.5 deg^2, the pixel scale is 8.0 arcsec, and the FWHM is ∼2 pixels. ASAS-SN nominally saturates at ∼10–11 mag, but light curves of saturated sources are sometimes quite good due to corrections made for bleed trails (see Kochanek et al. 2017).

The light curves for these sources were extracted as described in Jayasinghe et al. (2018a) using image subtraction (Alard & Lupton 1998; Alard 2000) and aperture photometry on the subtracted images with a 2 pixel radius aperture. The APASS catalogue was used for calibration. The zero-point offsets between the different cameras were corrected as described in Jayasinghe et al. (2018a).

Fig. 1 illustrates the relationship between the measured mean ASAS-SN *V*-band magnitudes and the APASS DR9 *V*-band magnitudes. Sources with $V_{\rm mean} \lesssim 14$ mag have similar *V*-band magnitudes, but a large fraction of the sources with $V_{\rm mean} \gtrsim 14$ mag show a discrepancy between the ASAS-SN and APASS measurements. This is due to blending in fields with significant stellar densities [i.e. the Large Magellanic Cloud (LMC) in this work]. The relatively large ASAS-SN pixel scale of 8.0 arcsec as compared to the smaller

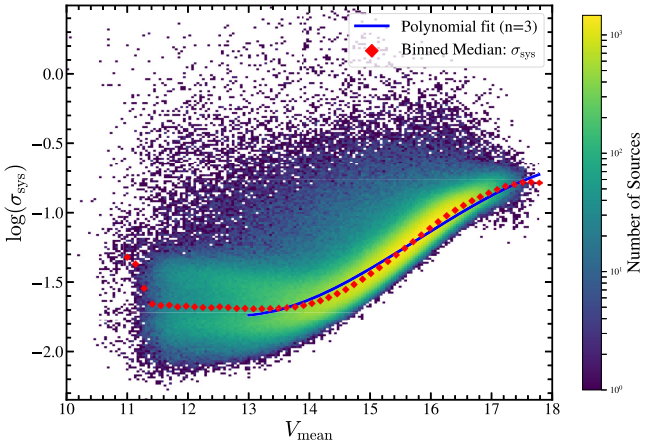

Figure 2. The distribution of σ_{sys} for the ∼1.3M sources. The red points are the binned median values of σ_{sys} for this sample in bins of ∼0.25 mag. The blue curve shows a third-order polynomial model for sources with $V >$ 13 mag (equation 3).

APASS pixel scale of 2.6 arcsec makes ASAS-SN photometry more susceptible to blending. Thus, ASAS-SN *V*-band measurements are systematically brighter for most sources in the LMC due to blended light.

The light-curve extraction provides a statistical error estimate, but the scatter in the light curves of apparently non-variable sources is generally larger than expected given the nominal statistical uncertainties. In Jayasinghe et al. (2018a), we used the reduced χ^2 statistic,

$$\frac{\chi^2}{N_{DOF}} = \frac{1}{N-1}\sum_{i=1}^{N}\left(\frac{V_i - V_{mean}}{\sigma(V_{mean})}\right)^2 \approx 1\,, \quad (1)$$

where V_i is the *V*-band magnitude for epoch i and V_{mean} is the mean *V*-band magnitude to determine the typical total uncertainty $\sigma(V_{mean})$ as a function of magnitude. In this work, we update our approach to estimating the systematic uncertainties in the ASAS-SN photometry.

We can view the photometric errors as the quadrature sum of the estimated statistical uncertainty σ_{stat} and a systematic σ_{sys}, with

$$\sigma^2 = \sigma_{sys}^2 + \sigma_{stat}^2\,. \quad (2)$$

We can measure σ as the rms scatter in the light curves of non-variable stars and then subtract the estimated statistical errors to derive σ_{sys}, with the results shown in Fig. 2 for the 1.3M sources in our sample. For sources with $V_{mean} < 13$ mag, the photometric uncertainties approach an ASAS-SN error floor of ∼0.02 mag. For the sources with $V_{mean} > 13$ mag, we fit a third-order polynomial,

$$\log\sigma_{sys} = A(x-13)^3 + B(x-13)^2 + C(x-13) - 1.738\,, \quad (3)$$

with $A = -1.03 \times 10^{-2}$, $B = 8.6 \times 10^{-2}$, and $C = 3.6 \times 10^{-2}$ to the median of the σ_{sys} versus V_{mean} distribution. The polynomial smoothly joins to 0.02 mag at $V = 13$ mag. To correct the errors in the light curves, we replace the formal magnitude errors by using equation (2) and either equation (3) or 0.02 mag for σ_{sys}.

We also identified a systematic issue that affects the light curves of certain sources due to malfunctioning shutters. The shutters in the ASAS-SN cameras periodically start to fail. Degraded shutters do not close completely, and stray light from neighbouring bright sources can impart trails on the images during readout (Fig. 3). This systematic is illustrated in the light curve for the non-variable source

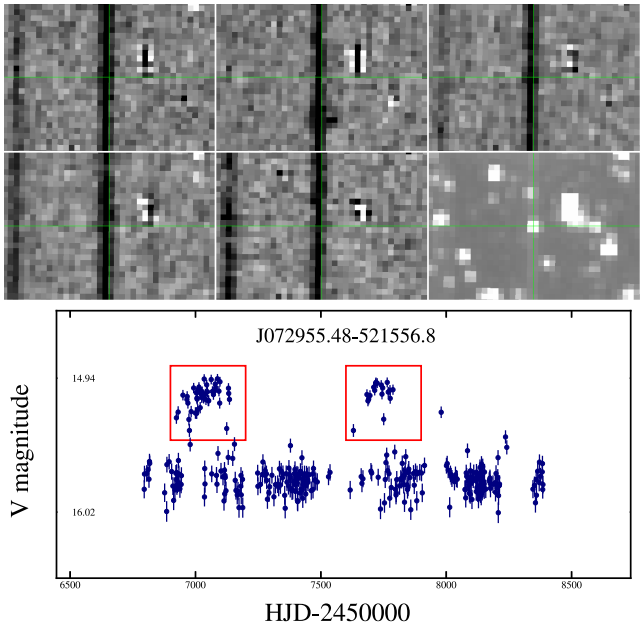

Figure 3. *Top*: examples of images that are affected by a malfunctioning shutter for the non-variable source J072955.48−521556.8, with the reference image shown in the bottom right. *Bottom*: the light curve for the source J072955.48−521556.8 with the affected epochs highlighted by the red boxes.

J072955.48−521556.8 (Fig. 3). We see that after the malfunctioning shutter is replaced, the light curve returns to normal, but after ∼700 d, the shutter begins to fail again. Some fraction of our ASAS-SN light curves will be affected by this systematic.

3 VARIABILITY ANALYSIS

Here we describe the procedure we used to identify and characterize variables in the source list. We describe how we cross-matched the APASS sources to external catalogues in Section 3.1. In Section 3.2, we describe the procedure we took to identify candidate variable sources. In Section 3.3, we discuss the application of the V2 random forest classifier model from Jayasinghe et al. (2018b) to classify these variables, and in Section 3.4, we discuss the corrections done to mitigate the effects of blending on the candidate variables.

3.1 Cross-matches to external catalogues

We identify cross-matches to the APASS sources with *Gaia* DR2 (Gaia Collaboration 2018a) using the pre-computed cross-matches from Marrese et al. (2019). The sources were also cross-matched to the probabilistic distance estimates from Bailer-Jones et al. (2018). We also cross-match the sources with 2MASS (Skrutskie et al. 2006) and AllWISE (Wright et al. 2010; Cutri et al. 2013) using a matching radius of 10.0 arcsec. We used TOPCAT (Taylor 2005) to cross-match the APASS sources with the 2MASS and AllWISE catalogues.

The LMC lies within the *TESS* southern CVZ. We used *Gaia* DR2 (Gaia Collaboration 2018c) to identify ∼119 000 sources from our source list that are LMC members. For sources in the LMC, we use a distance of $d = 49.97$ kpc (Pietrzyński et al. 2013) in our variability classifier.

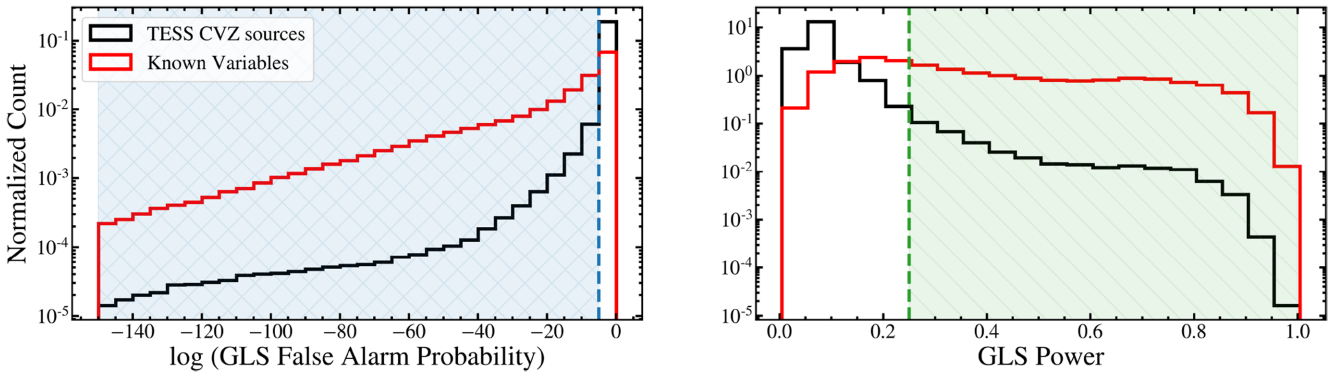

Figure 4. The distribution of the GLS false alarm probability (left), and the distribution of GLS power (right) for the ∼1.3M sources (black) and the set of known variables from Jayasinghe et al. (2018b) (red). Variable candidates had to lie in the shaded regions with log(FAP) < -10 and GLS Power > 0.25.

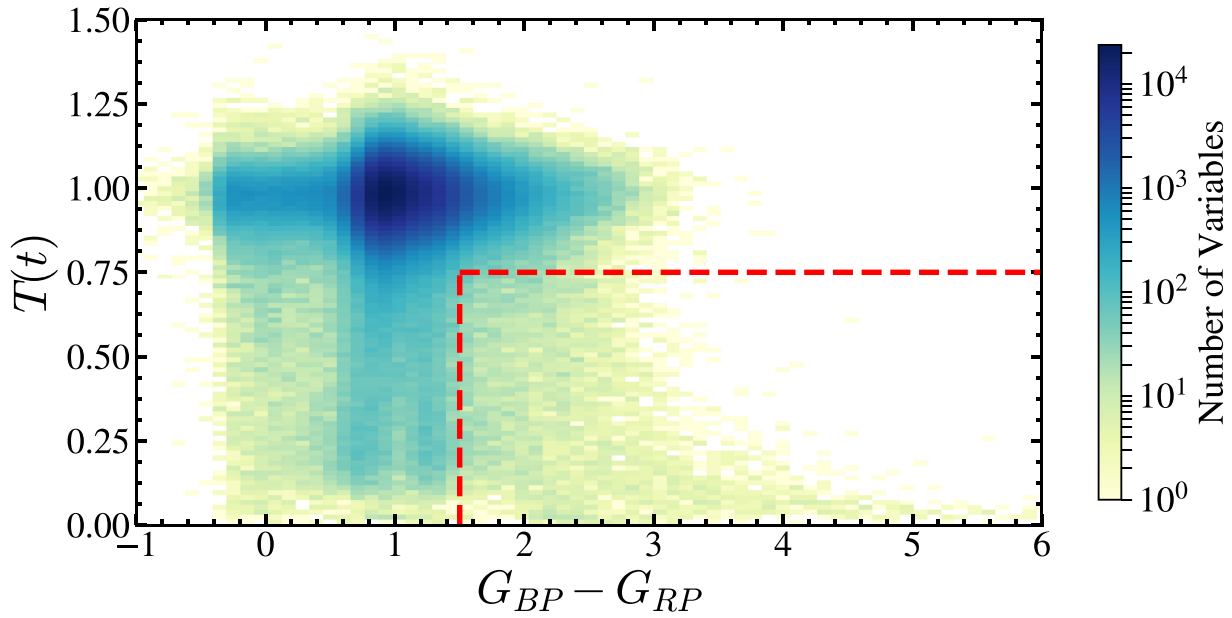

Figure 5. The distribution of $G_{BP} - G_{RP}$ with $T(t)$ for the ∼1.3M sources. The red shaded box encloses the sources that meet the criteria of $T(t) < 0.75$ and $G_{BP} - G_{RP} > 1.5$ mag used to identify red variable sources.

3.2 Variability cut-offs

There are numerous methods to identify variable sources from a sample of light curves. The most commonly used method involves correlating the variations observed in multiple bands to pick out 'true' variables from the false positives (Stetson 1996). The ASAS-SN observations used in this work are made with a single filter, which makes the use of multiband variability statistics impossible. In this work, we used several methods, including periodogram statistics, light-curve features, and external photometry to identify variable sources.

We used the ASTROPY implementation of the generalized Lomb–Scargle (GLS; Scargle 1982; Zechmeister & Kürster 2009) periodogram to search for periodicity over the range $0.05 \leq P \leq 1000$ d for each of the ∼1.3M sources. We utilize the false alarm probability (FAP) and the power of the best GLS period as means of identifying significantly periodic sources. Sources with log(FAP) < -10 and GLS Power > 0.25 were selected for further analysis (Fig. 4).

We calculated the Lafler–Kinmann (Lafler & Kinman 1965; Clarke 2002) string length statistic $T(t)$ on the temporal light curve using the definition

$$T(t) = \frac{\sum_{i=1}^{N}(m_{i+1} - m_i)^2}{\sum_{i=1}^{N}(m_i - \overline{m})^2} \times \frac{(N-1)}{2N} \quad (4)$$

from Clarke (2002), where the m_i are the magnitudes sorted temporally and $\overline{m}$ is the mean magnitude. We can also calculate this statistic sorting the light curve based on phase for a given period, which we will call $T(\phi|P)$. To identify red variables, we empirically isolate sources with $T(t) < 0.75$ and the *Gaia* DR2 colour $G_{BP} - G_{RP} > 1.5$ mag (Fig. 5). Red variables typically have long periods that result in noticeable structure in their temporal light curves. This structure results in smaller values of $T(t)$ for the light curves of long-period variables when compared to sources with short-term variability (see Jayasinghe et al. 2018b).

We also compute the ratio of magnitudes brighter or fainter than average (A_{HL}; Kim & Bailer-Jones 2016; Jayasinghe et al. 2018b) for all the sources. We found in Paper II that eclipsing binaries have larger values of A_{HL} than most variables, so we flag sources with $A_{HL} > 1.5$ for further analysis. This variability

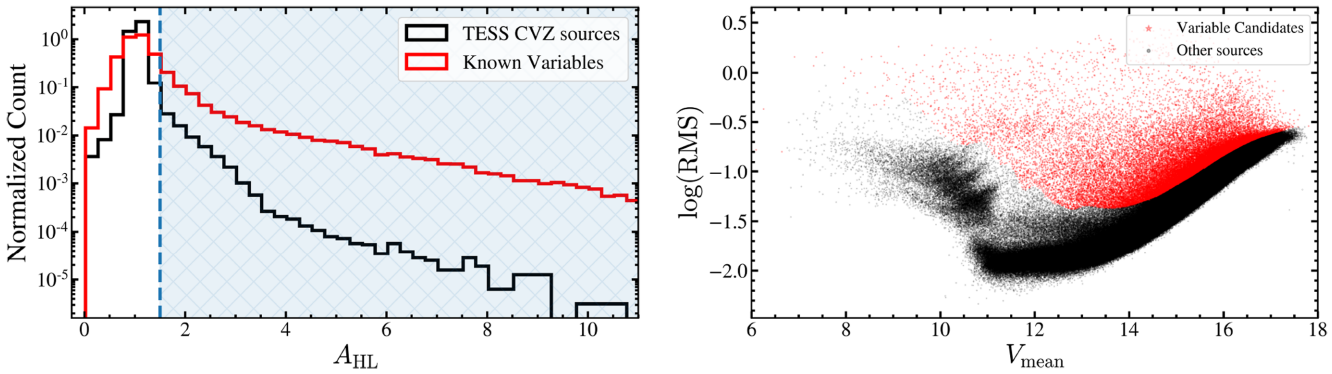

Figure 6. The distribution of $A_{\rm HL}$ (left), and the distribution of log RMS with mean magnitude (right) for the ∼1.3M sources. The sources with $A_{\rm HL} > 1.5$ are shaded in blue and the sources with log RMS > 95th percentile in each magnitude bin are shaded in red. The distribution of $A_{\rm HL}$ for the set of known variables from Jayasinghe et al. (2018b) is plotted in red.

Table 1. Summary of the variability selection cuts.

Variable(s)	Cut	Used to identify	Sources
GLS power	>0.25	Periodic Variables	24257
GLS log (FAP)	<−10	Periodic Variables	39761
$G_{BP} - G_{RP}$ and $T(t)$	>1.5 AND <0.75	Red Variables	7741
$A_{\rm HL}$	>1.5	Eclipsing Binaries	20864
log (RMS)	>95$^{\rm th}$percentile	Large variations	45486

cut is expected to improve the identification of detached eclipsing binaries. We also identify sources with a light-curve RMS larger than the 95th percentile for the other stars in magnitude bins of 0.25 mag (Fig. 6) in order to select sources with significant flux variations.

The variability cuts and the number of variable candidates isolated through each cut are summarized in Table 1. The combination of these cuts helps identify different variable sources and increase our completeness when compared to relying on just one or two parameters. Through these variability cut-offs, we identified ∼60 000 unique candidates. This amounts to ∼5 per cent of the sources on the initial list.

3.3 Variability classification

We derived periods for the ∼60 000 variable candidates following the procedure described in Jayasinghe et al. (2018a,b). The `astrobase` implementation (Bhatti et al. 2018) of the GLS (Scargle 1982; Zechmeister & Kürster 2009), the multiharmonic analysis of variance (Schwarzenberg-Czerny 1996), and the box least squares (Kovács, Zucker & Mazeh 2002) periodograms were used to search for periodicity in these light curves. For each periodic source, we calculate the improvement in the Lafler–Kinmann string length statistic when phased with the best period ($T(\phi|P)$) when compared to the string length statistic calculated on the temporal light curve ($T(t)$),

$$\delta = \frac{T(\phi|P) - T(t)}{T(t)}. \quad (5)$$

Following the period search, we use the variability classifier implemented in Jayasinghe et al. (2018b) to classify these variable candidates. We choose to visually review the classifications in order to improve our catalogue. For the visual review, we select the sources with periods $P < 40$ d if $\delta < 0.05$ AND $T(t) < 0.75$. The majority of the periodic variables within this period range should show significant improvements in the string length statistic when phased with a period. Sources with $P > 40$ d are selected if they have $T(t) < 1$. All irregular and aperiodic sources are also selected for visual review. In total, we visually reviewed ∼23 000 variable candidates. During the process of visual review, we identified incorrect classifications (3 per cent) and periods (4 per cent) and corrected them. Sources with significant systematic and spurious variability were removed (46 per cent). We also changed the classifications of ∼1300 (6 per cent) sources to the generic variability type ('VAR'). At this stage, our list of variables consisted of ∼12 300 sources. This means that our initial candidate list had a false positive rate of ∼80 per cent. Part of this is that we were deliberately generous in our initial selection so that we can use the results to improve this aspect of the pipeline as we progress with our effort to identify variable sources over the full sky.

3.4 Blending corrections

The large pixel scale of the ASAS-SN images (8.0 arcsec) and the FWHM (∼16.0 arcsec) results in blending towards crowded regions. The APASS catalogue was constructed with images that have a significantly smaller pixel scale (2.6 arcsec), and as a result of this, multiple APASS sources can fall into a single ASAS-SN pixel. We do not correct for the contaminating light in the photometry of the blended sources, but we identify and correct blended variable groups in our catalogue.

Since we extracted light curves for the positions of APASS sources, we can have two or more such sources inside a single ASAS-SN resolution element. If we select the sources with another APASS neighbour within 30.0 arcsec, we find that 559 of the ∼12 300 variables had a neighbour within 30.0 arcsec. We compute the flux variability amplitudes for these sources using a random forest regression model (Jayasinghe et al. 2018b). The majority of the variable groups consisted of two sources, with a few groups consisting of up to three sources. For each variable group, we

Table 2. Variables by type.

VSX type	Description	LMC	Not LMC	New discoveries
CWA	W Virginis type variables with $P > 8$ d	10	–	1
CWB	W Virginis type variables with $P < 8$ d	4	8	2
DCEP	Fundamental mode Classical Cepheids	577	12	12
DCEPS	First overtone Cepheids	280	9	10
DSCT	δ Scuti variables	–	44	42
EA	Detached Algol-type binaries	103	1109	865
EB	β Lyrae type binaries	129	523	353
EW	W Ursae Majoris type binaries	97	1961	1228
ELL	Ellipsoidal variables	1	11	12
HADS	High-amplitude δ Scuti variables	–	102	61
ROT	Rotational variables	–	881	813
RRAB	RR Lyrae variables (type ab)	42	444	44
RRC	First overtone RR Lyrae variables	4	443	217
RRD	Double-mode RR Lyrae variables	–	4	3
RVA	RV Tauri variables (subtype A)	9	1	1
SR	Semiregular variables	1017	1487	1340
L	Irregular variables	298	137	262
GCAS	γ Cassiopeiae variables	191	49	128
YSO	Young stellar objects	2	8	6
ROT:	Uncertain rotational variables	–	186	174
DSCT:	Uncertain δ Scuti variables	4	63	48
GCAS:	Uncertain γ Cassiopeiae variables	10	–	3
VAR	Generic variables	40	1390	1385

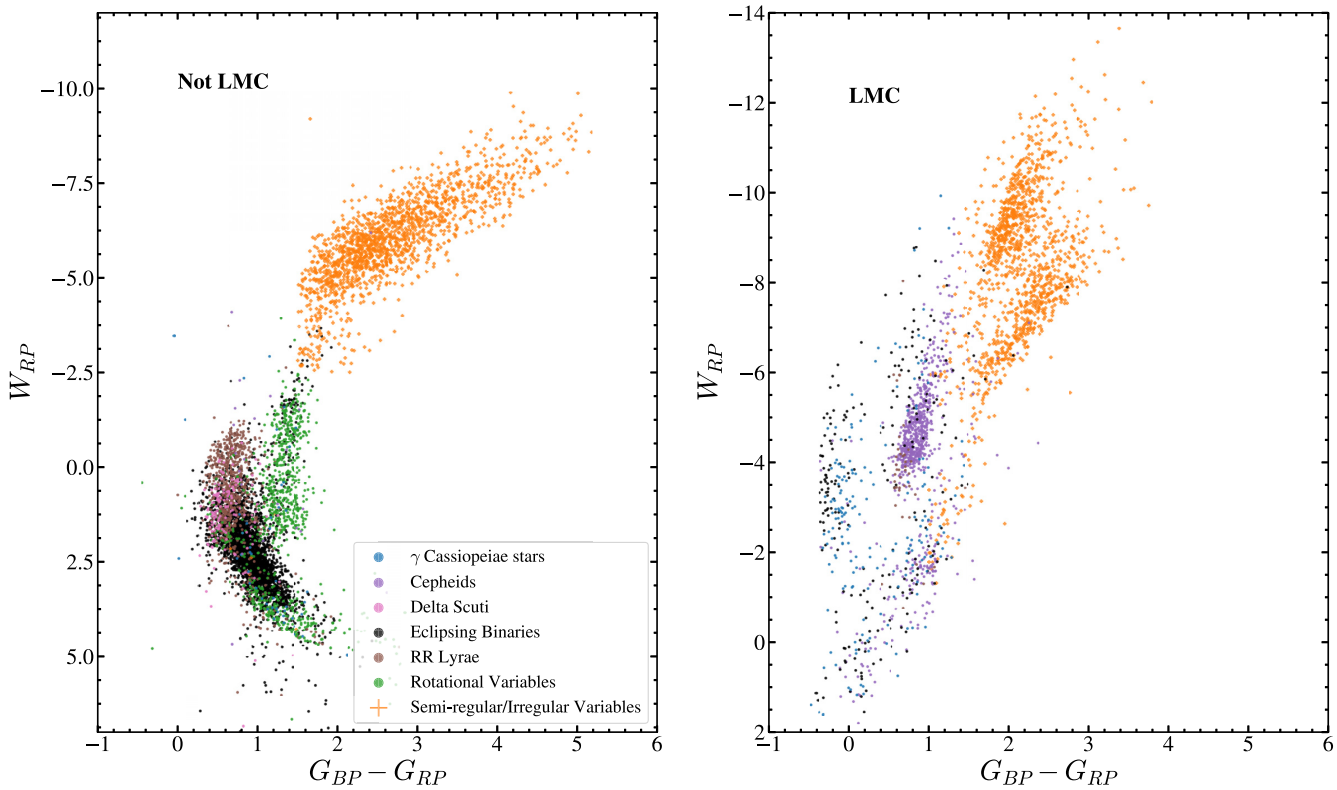

Figure 7. The Wesenheit W_{RP} versus $G_{BP} - G_{RP}$ colour–magnitude diagram for the variables, outside the LMC (left) and in the LMC (right).

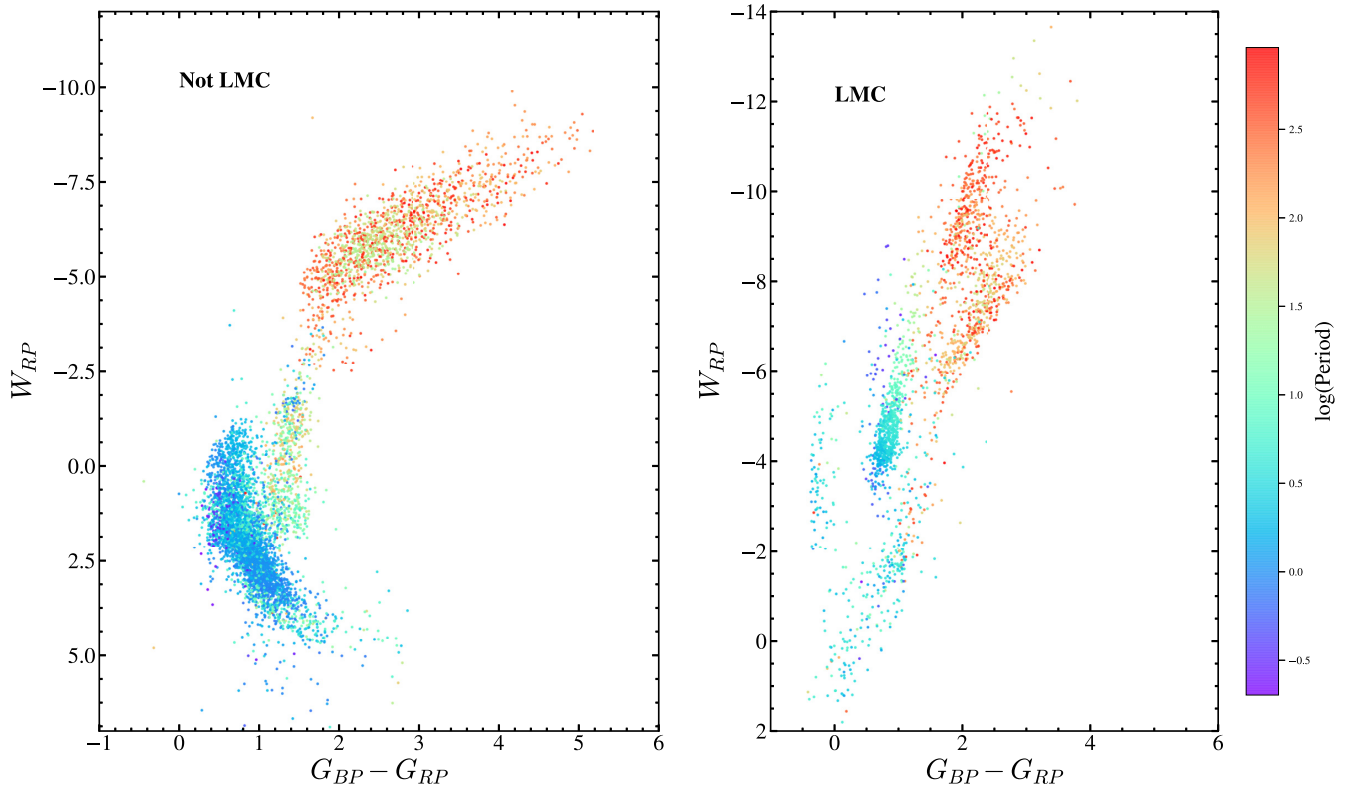

Figure 8. The Wesenheit W_{RP} versus $G_{BP} - G_{RP}$ colour–magnitude diagram for the periodic variables, outside the LMC (left) and in the LMC (right). The points are coloured by the period.

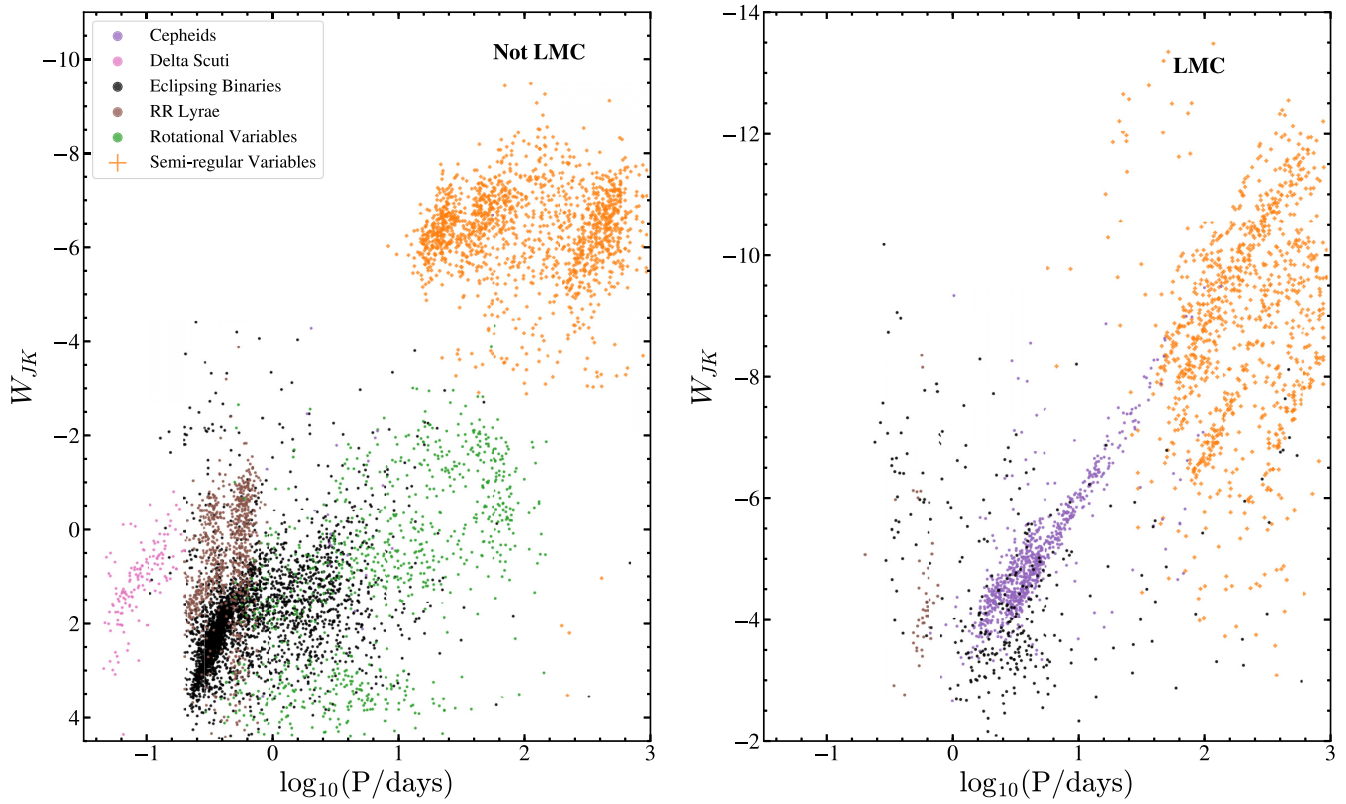

Figure 9. The Wesenheit W_{JK} PLR diagram for the periodic variables, outside the LMC (left) and in the LMC (right). The points are coloured as in Fig. 7.

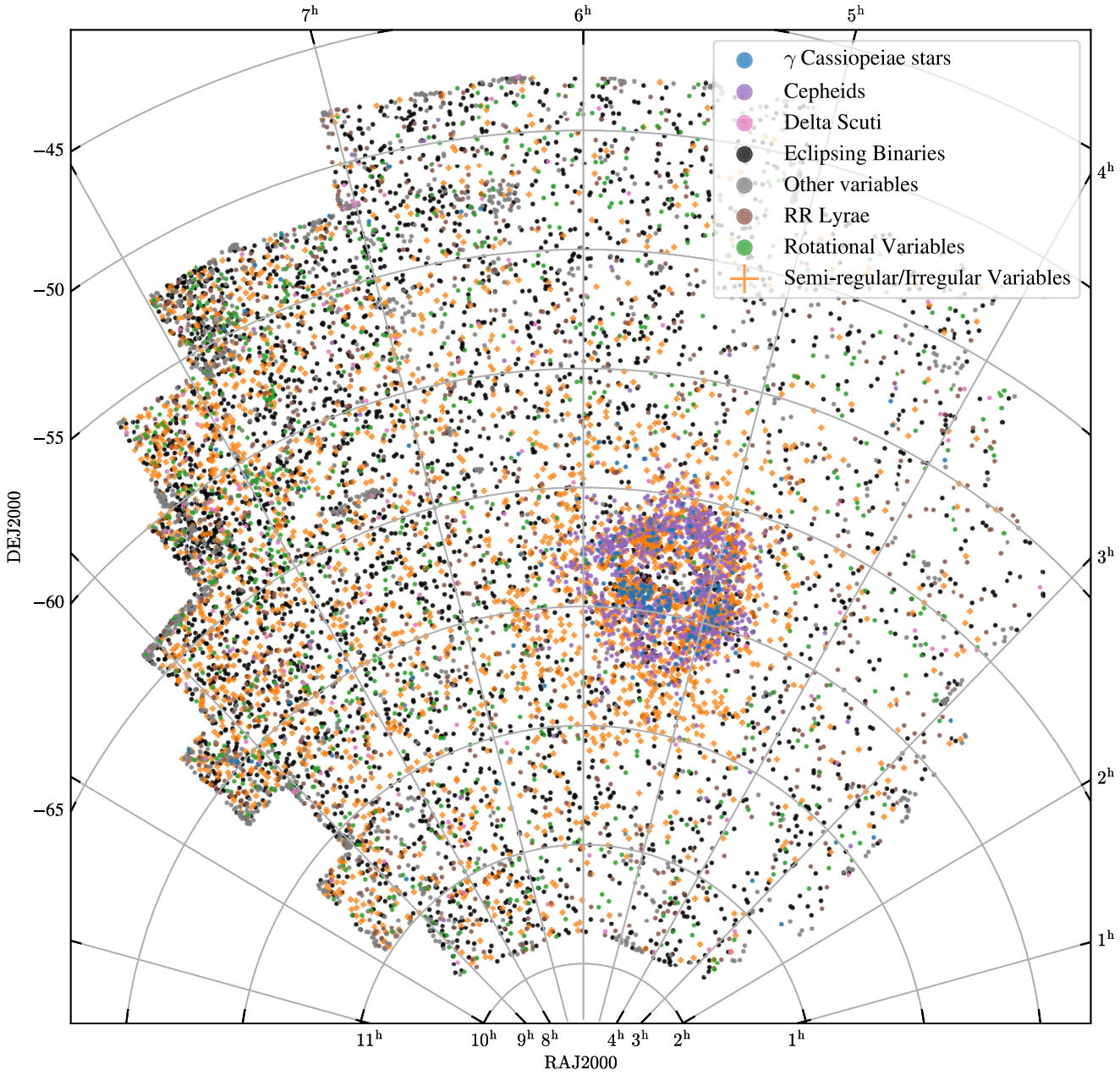

Figure 10. The sky distribution of the variables in equatorial coordinates. The points are coloured as in Fig. 7.

consider the source with the largest flux variability as the 'true' variable, and remove the other overlapping sources from the final list. Following this treatment, our list of variables consisted of ∼11 700 sources.

4 RESULTS

The complete catalogue of ∼11 700 variables is available at the ASAS-SN Variable Stars Database (https://asas-sn.osu.edu/variables) along with the *V*-band light curves for each source. Table 2 lists the number of sources of each variability type in the catalogue.

In Paper II, we used the reddening-free Wesenheit magnitudes (Madore 1982; Lebzelter et al. 2018)

$$W_{RP} = M_{G_{RP}} - 1.3(G_{BP} - G_{RP}), \quad (6)$$

and

$$W_{JK} = M_{K_s} - 0.686(J - K_s) \quad (7)$$

for variability classification. The Wesenheit W_{RP} versus $G_{BP} - G_{RP}$ colour–magnitude diagram for all the variables is shown in Fig. 7. We have sorted the variables into groups to highlight the different classes of variable sources. Owing to the magnitude limit of ASAS-SN, we are only able to detect sufficiently bright sources ($V \lesssim 16$ mag, $W_{RP} \lesssim 1.5$ mag) in the LMC. This is evident in the Wesenheit colour–magnitude diagram for the LMC sources. For the sources outside the LMC, we probe a wider range of magnitudes ($W_{RP} \lesssim 6$ mag), including RR Lyrae, rotational variables, and δ Scuti variables.

We have also plotted the Wesenheit W_{RP} versus $G_{BP} - G_{RP}$ colour–magnitude diagram for all the periodic variables in Fig. 8,

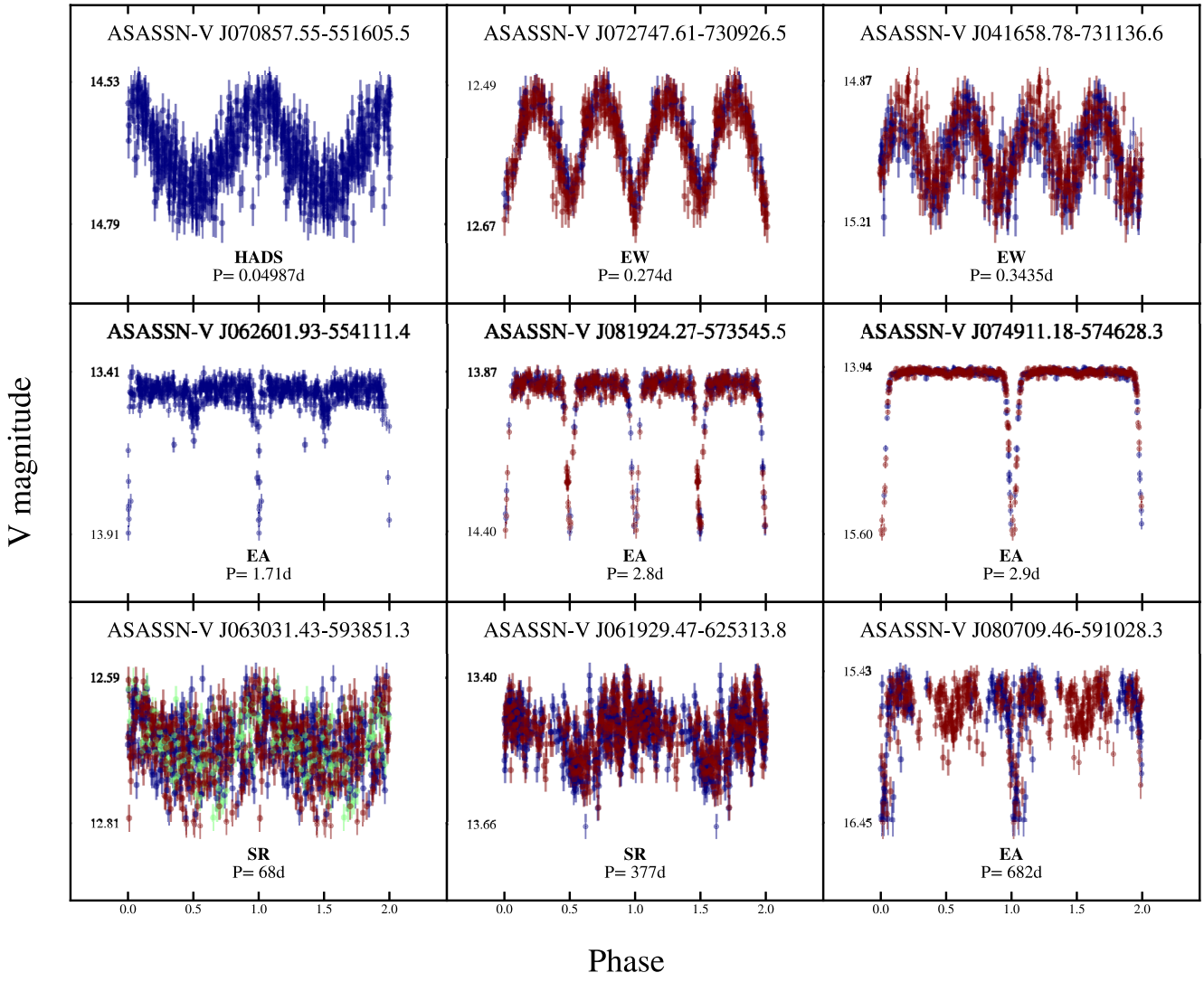

Figure 11. Phased light curves for examples of the newly discovered periodic variables. The light curves are scaled by their minimum and maximum *V*-band magnitudes. Different coloured points correspond to data from the different ASAS-SN cameras. The different variability types are defined in Table 2.

with the points coloured according to the period. This essentially highlights the large dynamic range in period probed by the ASAS-SN light curves.

We note that the identification of Mira variables in the LMC is hindered by blending. Due to blended light, the observed ASAS-SN amplitudes of these sources fall below the amplitude threshold of $V > 2$ mag that is used to define a Mira variable in our pipeline. In reality, some fraction of the LMC semiregular variables in this catalogue are actually Mira variables. From the sample of known semiregular variables in the LMC, we estimate that the fraction of Mira variables classified as semiregular variables is ∼23 per cent.

Using the same colour scheme, the combined Wesenheit W_{JK} period-luminosity relationship (PLR) diagram for the periodic variables is shown in Fig. 9. The PLR sequences for the Cepheids and semiregular variables in the LMC are well defined (Soszynski et al. 2005). Most of the eclipsing binaries identified in the LMC are either detached or semidetached systems, and do not follow the well-defined PLR for contact binaries that is observed in the PLR diagram for the sources outside the LMC.

We also show the sky distribution of the variables identified in this work in Fig. 10. We see that the distribution of eclipsing binaries and rotational variables (black points) is random, but the distribution of Cepheids is strongly clustered towards the LMC as is expected. We also note the clustering of semiregular/irregular variables (red giants) towards the LMC and the Galactic disc.

We matched our list of variables to the VSX (Watson, Henden & Price 2006) catalogue available in 2018 October, with a matching radius of 16.0 arcsec to identify previously discovered variables. The variables discovered by the All-Sky Automated Survey (ASAS; Pojmanski 2002) and the Catalina Real-Time Transient Survey (CRTS; Drake et al. 2014) are included in the VSX data base. We also match our variables to the catalogues of variable stars discovered by ASAS-SN (Jayasinghe et al. 2018a), the catalogues of variable stars in the Magellanic clouds and the Galactic bulge from the Optical Gravitational Lensing Experiment (OGLE; Udalski 2003; Pawlak et al. 2016; Soszyński et al. 2016, and references therein), the *Gaia* DR2 catalog of variables (Gaia Collaboration 2018a; Gaia Collaboration 2018b; Holl et al. 2018) , the catalogue of variables from the Asteroid Terrestrial-impact Last Alert System (ATLAS; Heinze et al. 2018; Tonry et al. 2018), the catalogue of KELT variables (Oelkers et al. 2018), and the variables from MACHO (Alcock et al. 1997). Of the ∼11 700 variables identified

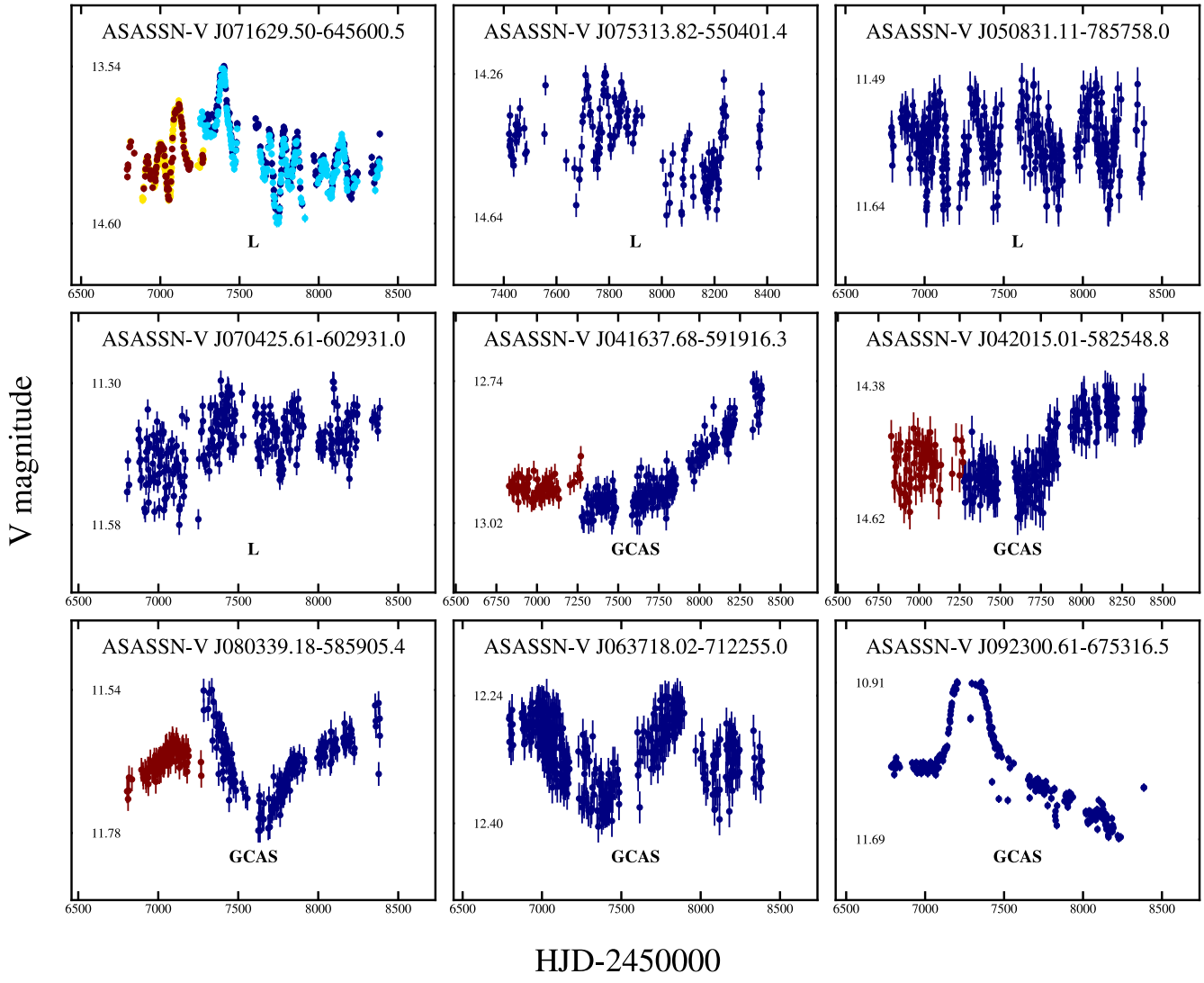

Figure 12. Light curves for examples of the newly discovered irregular variables. The format is the same as for Fig. 11.

in this work, ∼4700 were previously discovered by other surveys, as also listed in Table 2. The majority of these known variables consist of eclipsing binaries (∼31 per cent), irregular/semiregular variables (∼28 per cent), and Cepheids (∼19 per cent).

This leaves ∼7000 new variables. Most of the new discoveries are eclipsing binaries (∼35 per cent) and irregular/semiregular variables (∼23 per cent). Example light curves for the newly discovered periodic variables are shown in Fig. 11. We also discovered 128 new GCAS variables, 81 of which are located in the LMC. GCAS variables are rapidly rotating early-type irregular variable stars (typically Be stars) with mass outflow from their equatorial regions. Example light curves for the newly identified GCAS variables are shown in Fig. 12.

We also discovered another long-period detached eclipsing binary (ASASSN-V J080709.46−591028.3) in this work. ASASSN-V J080709.46−591028.3 is located away from the LMC and has an orbital period of $P_{\rm orb}$ ∼ 682 d (∼1.9 yr). Its light curve shows evidence of both a primary and a secondary eclipse with a primary eclipse depth of ∼1 mag (Fig. 11).

A non-negligible fraction of these new discoveries were classified as generic variables (∼20 per cent). These are mostly low-amplitude or faint sources. Example light curves are shown for a subset of the newly discovered periodic and irregular variables in Figs 11 and 12.

5 CONCLUSIONS

We systematically searched for variable sources in a ∼1000 deg^2 region surrounding the Southern Ecliptic Pole. This region is coincident with the southern continuous viewing zone for the *TESS* satellite and thus, a large majority of these sources will have excellent *TESS* light curves.

Through our search, we identified ∼11 700 variable sources, of which ∼7 000 are new discoveries. Variable sources identified in the LMC largely consist of luminous variables, including Cepheids, GCAS variables (Be stars), and red giants. We identify a broader sample of variables outside the LMC, including RR Lyrae, eclipsing binaries, rotational variables, and δ Scuti variables.

We have developed a user-friendly interface to retrieve pre-computed ASAS-SN *V*-band light curves for APASS sources. The *V*-band light curves of all the ∼1.3M sources studied in this work are available online at the ASAS-SN Photometry Database (https://asas-sn.osu.edu/photometry). To highlight the possible blended sources, a flag is assigned to each source if the distance to the

nearest APASS neighbour is <16.0 arcsec. The new variable sources have also been added to the ASAS-SN variable stars data base (https://asas-sn.osu.edu/variables).

As part of our ongoing effort to systematically analyse all the ∼50 million $V < 17$ mag APASS sources for variability, we will gradually update this data base with the light curves for the sources across the remainder of the sky over the course of 2019. This work provides long-baseline *V*-band light curves for a large fraction of the sources in the *TESS* southern CVZ and is a useful supplement to the short-baseline *TESS* light curves that possess better photometric precision.

ACKNOWLEDGEMENTS

We thank the referee for their useful comments. We thank the Las Cumbres Observatory and its staff for its continuing support of the ASAS-SN project. We also thank the Ohio State University College of Arts and Sciences Technology Services for helping us set up and maintain the ASAS-SN variable stars and photometry data bases.

ASAS-SN is supported by the Gordon and Betty Moore Foundation through grant GBMF5490 to the Ohio State University and NSF grant AST-1515927. Development of ASAS-SN has been supported by NSF grant AST-0908816, the Mt. Cuba Astronomical Foundation, the Center for Cosmology and AstroParticle Physics at the Ohio State University, the Chinese Academy of Sciences South America Center for Astronomy (CAS-SACA), the Villum Foundation, and George Skestos.

This work is supported in part by Scialog Scholar grant 24216 from the Research Corporation. TAT acknowledges support from a Simons Foundation Fellowship and from an IBM Einstein Fellowship from the Institute for Advanced Study, Princeton. Support for JLP is provided in part by the Ministry of Economy, Development, and Tourism's Millennium Science Initiative through grant IC120009, awarded to The Millennium Institute of Astrophysics, MAS. SD acknowledges Project 11573003 supported by NSFC. Support for MP and OP has been provided by the PRIMUS/SCI/17 award from Charles University. This work was partly supported by NSFC 11721303.

This work has made use of data from the European Space Agency (ESA) mission *Gaia* (https://www.cosmos.esa.int/gaia), processed by the *Gaia* Data Processing and Analysis Consortium. This publication makes use of data products from the Two Micron All Sky Survey, as well as data products from the Wide-field Infrared Survey Explorer. This research was also made possible through the use of the AAVSO Photometric All-Sky Survey (APASS), funded by the Robert Martin Ayers Sciences Fund.

This research has made use of the VizieR catalogue access tool, CDS, Strasbourg, France. This research also made use of ASTROPY, a community-developed core PYTHON package for Astronomy (Astropy Collaboration 2013).

REFERENCES

Alard C., 2000, A&AS, 144, 363
Alard C., Lupton R. H., 1998, ApJ, 503, 325
Alcock C. et al., 1997, ApJ, 486, 697
Astropy Collaboration et al., 2013, A&A, 558, A33
Bailer-Jones C. A. L., Rybizki J., Fouesneau M., Mantelet G., Andrae R., 2018, AJ, 156, 58
Beaton R. L. et al., 2018, Space Sci. Rev., 214, 113
Bhatti W. et al., 2018, astrobase, v0.3.8, Zenodo, http://doi.org/10.5281/zenodo.1185231
Brown T. M. et al., 2013, PASP, 125, 1031
Brown J. S. et al., 2019, MNRAS, 484, 3785
Clarke D., 2002, A&A, 386, 763
Cutri R. M. et al., 2013, VizieR Online Data Catalog, 2328
Derue F. et al., 2002, A&A, 389, 149
Drake A. J. et al., 2014, ApJS, 213, 9
Feast M., Whitelock P. A., 2014, in Proc. IAU Symp. 298, Setting the Scene for Gaia and LAMOST. Cambridge Univ. Press, Cambridge, p. 40
Gaia Collaboration Brown A. G. A., et al., 2018a, A&A, 616, A1
Gaia Collaboration Eyer L., Rimoldini L. et al., 2018b, preprint (arXiv:1804.09382)
Gaia Collaboration Helmi A., et al., 2018c, A&A, 616, A12
Heinze A. N. et al., 2018, AJ, 156, 241
Henden A. A., Levine S., Terrell D., Welch D. L., 2015, American Astronomical Society Meeting Abstracts #225, 336.16
Holl B. et al., 2018, A&A, 618, A30
Holoien T. W.-S. et al., 2014, MNRAS, 445, 3263
Holoien T. W.-S. et al., 2016, MNRAS, 455, 2918
Holoien T. W.-S. et al., 2017, MNRAS, 471, 4966
Holoien T. W.-S. et al., 2018, preprint (arXiv:1808.02890)
Holoien T. W.-S. et al., 2019, MNRAS, 484, 1899
Holtzman J. A. et al., 2015, AJ, 150, 148
Jayasinghe T. et al., 2018, MNRAS, 477, 3145
Jayasinghe T. et al., 2018, preprint (arXiv:1809.07329)
Jayasinghe T. et al., 2018, RNAA, 2, 181
Jayasinghe T. et al., 2018, RNAA, 2, 125
Kim D.-W., Bailer-Jones C. A. L., 2016, A&A, 587, A18
Kochanek C. S. et al., 2017, PASP, 129, 104502
Kovács G., Zucker S., Mazeh T., 2002, A&A, 391, 369
Lafler J., Kinman T. D., 1965, ApJS, 11, 216
Leavitt H. S., 1908, AnHar, 60, 87
Lebzelter T., Mowlavi N., Marigo P., Pastorelli G., Trabucchi M., Wood P. R., Lecoeur-Taibi I., 2018, A&A, 616, L13
Madore B. F., 1982, ApJ, 253, 575
Marrese P. M., Marinoni S., Fabrizio M., Altavilla G., 2019, A&A, 621, A144
Matsunaga N., 2018, in Proc. IAU Symp. 334, Rediscovering our Galaxy. Cambridge Univ. Press, Cambridge, p. 57
Matsunaga N. et al., 2006, MNRAS, 370, 1979
Oelkers R. J. et al., 2018, AJ, 155, 39
Pawlak M. et al., 2016, Acta Astron., 66, 421
Pietrzyński G. et al., 2013, Nature, 495, 76
Pojmanski G., 2002, Acta Astron., 52, 397
Ricker G. R. et al., 2015, JATI, 1, 014003
Rodríguez R. et al., 2018, RNAA, 2, 8
Scargle J. D., 1982, ApJ, 263, 835
Schmidt S. J. et al., 2018, preprint (arXiv:1809.04510)
Schwarzenberg-Czerny A., 1996, ApJ, 460, L107
Shappee B. J. et al., 2014, ApJ, 788, 48
Shields J. V. et al., 2019, MNRAS, 483, 4470
Skrutskie M. F. et al., 2006, AJ, 131, 1163
Soszynski I. et al., 2005, Acta Astron., 55, 331
Soszyński I. et al., 2016, Acta Astron., 66, 405
Stassun K. G. et al., 2018, AJ, 156, 102
Stetson P. B., 1996, PASP, 108, 851
Taylor M. B., 2005, in ASP Conf. Ser. Vol. 347, Astronomical Data Analysis Software and Systems XIV, Astron. Soc. Pac., San Francisco, p. 29
Thompson T. A. et al., 2018, preprint (arXiv:1806.02751)
Tonry J. L. et al., 2018, PASP, 130, 064505
Torres G., Andersen J., Giménez A., 2010, A&AR, 18, 67
Tucker M. A. et al., 2018, ApJ, 867, L9
Udalski A., 2003, Acta Astron., 53, 291
Watson C. L., Henden A. A., Price A., 2006, SASS, 25, 47
Woźniak P. R. et al., 2004, AJ, 127, 2436
Wright E. L. et al., 2010, AJ, 140, 1868
Zechmeister M., Kürster M., 2009, A&A, 496, 577

This paper has been typeset from a TEX/LATEX file prepared by the author.